Control-based Design of a Five-bar Mechanism

L. Kaci[1,2], S. Briot[1], C. Boudaud[3] and P. Martinet[1,2]

[1]*IRCCyN, UMR CNRS 6597, France*   [2]*École Centrale de Nantes, France*
e-mail: {kaci,briot,martinet}@irccyn.ec-nantes.fr
[3]*LIMBHA, Goupe École Supérieure du Bois, France,*
e-mail: clement.boudaud@ecoledubois.fr

Abstract. To ensure optimal performance of parallel robots, a rigorous design process has to be implemented. However, this may not be enough due to the presence of complex phenomena such as vibration, clearance, deformation, hard to model and thus to control, but considerably impacting the robot performance.

An efficient approach to improve performance via bypassing the modeling issues is the use of exteroceptive sensors to estimate the end-effector pose. Any external observation, however, impacts the robot performance. It is thus necessary to optimize the robot design with respect to (usual) mechanical performance criteria, but also with respect to performance indices coming from the definition of the sensor-based controller. Thus it is necessary to achieve control-based design.

In this work, a five-bar mechanism is optimized using a classical design methodology. The robot is then compared with other designs which are the result of a new methodology, taking into account the nature of the desired control scheme through the incorporation of control-based performance indices into the optimization process. Though the latter designs may have a bigger footprint, they will prove to exhibit better accuracy performance when controlled using exteroceptive sensors.

Key words: Five-bar mechanism, control-based design, visual-servoing, optimal design.

1 Introduction

Compared to serial robots, parallel kinematic manipulators are stiffer and can reach higher speeds and accelerations [13]. However, their control is troublesome because of the complex mechanical structure, highly coupled joint motions and many other factors (e.g. clearances, assembly errors, etc.) which degrade stability and accuracy.

When the robot specifications include high accuracy, it is important to use detailed models during the design stage, which take into account deformations, clearance and vibrations. However, even detailed models suffer from inaccuracy when they are implemented, due to several factors (e.g. manufacturing and assembly errors). To make sure that the finished product corresponds to the designed models, the (in-line or off-line) identification of several parameters must be performed [11], which in the case of mass-produced robots can be costly and time-consuming. Moreover, some effects may still not be compensated, such as clearance.

One efficient way to overcome this complexity is to use an external measure for the control of the robot, bypassing the modeling issues. Sensor-based control approaches have proven to be more efficient than their model-based counterparts when accuracy is required in robotized industrial applications [7].

When using external sensors for control, it is important to choose (a) an appropriate set of sensors combined with (b) appropriate observed features. The most
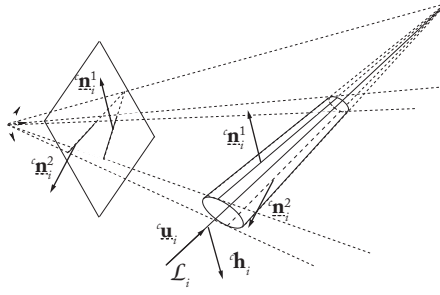
Fig. 1 Projection of a cylinder in the image

common approach consists of the direct observation of the end-effector pose [14]. In some cases, however, it may be difficult or unwise to observe the end-effector of the robot, e.g. in the case of a milling operation. Another approach is the observation of the legs [1, 2] from which the end-effector pose can be easily reconstructed.

This last approach was promising. However, it was proven in [5] that using vision for the observation of the robot legs introduced a mapping which is not free of singularity. These singularities can be found through the observation that the aforementioned mapping coincides with the kinematics model of a virtual robot "hidden" within the controller. This hidden robot is indeed a tangible visualization of the mapping, and its performance impacts the real robot accuracy [4].

In the present paper, we propose to take into account the accuracy performance associated with different leg-based visual servoing techniques in order to optimally design a five-bar mechanism. The aim is to certify its accuracy performance in a prescribed workspace when it is controlled with the aforementioned leg-based servoing approaches. Results will be compared in terms of accuracy with a five-bar which is optimally designed without taking into account the controller performance.

2 Recalls on leg-based visual servoing of parallel robots

Leg-based visual servoing approaches are based on the fact that either the robot leg directions given by the unit vector $^c\underline{\mathbf{u}}_i$ or the lines $\mathscr{L}_i$ passing through the robot links[1] which are defined using the Plücker coordinates ($^c\underline{\mathbf{u}}_i$, $^c\mathbf{h}_i$) (Fig. 1) are controlled instead of the usual actuator encoder positions $\mathbf{q}$.

As shown in [1], it is possible to control a parallel robot based on the observation of its legs because we can find some kinematic constraint relations between its end-effector pose (twist, resp.) and the vectors $^c\underline{\mathbf{u}}_i$ and $^c\mathbf{h}_i$ (their derivatives with respect to time, resp.). From [1, 15], we know that the leg velocities can be linked to the platform twist $^c\boldsymbol{\tau}_c$ through the use of an interaction matrix $\mathbf{M}_{ui}^T$ or $\mathbf{M}_{uhi}^T$ (depending on the controller) defined by (the superscript "c" denotes the camera frame):

---

[1] In the present paper, we consider that the robot links are cylindrical, which is the case for many parallel robots [13]. As a result, the lines passing through the links correspond to the cylinder axes.

$$^c\underline{\dot{\mathbf{u}}}_i = \mathbf{M}_{ui}^{T\,c}\boldsymbol{\tau}_c \text{ (in the case of a leg-direction-based controller [1])} \tag{1}$$

$$\begin{bmatrix} ^c\underline{\dot{\mathbf{u}}}_i^T & ^c\dot{\mathbf{h}}_i^T \end{bmatrix}^T = \mathbf{M}_{uhi}^{T\,c}\boldsymbol{\tau}_c \text{ (in the case of a line-based controller [15])} \tag{2}$$

where $\mathbf{M}_i^T$ is the interaction matrix for the leg i. $\mathbf{M}_{ui}^T$ is of dimension (3×6) with a rank $r \le 2$ while $\mathbf{M}_{uhi}^T$ is of dimension (6×6) with a rank $r \le 4$ [1, 15].

The values of $(^c\underline{\mathbf{u}}_i, {}^c\mathbf{h}_i)$ can be extracted from the projection of the cylindrical link in the image space (parameterized by the vectors $^c\underline{\mathbf{n}}_i^j$ in Fig. 1) [1, 15] while their derivative with respect to time can be obtained through the expressions:

$$^c\underline{\dot{\mathbf{u}}}_i = \mathbf{N}_i^T \begin{bmatrix} ^c\underline{\dot{\mathbf{n}}}_i^1 \\ ^c\underline{\dot{\mathbf{n}}}_i^2 \end{bmatrix}, \quad ^c\dot{\mathbf{h}}_i = \mathbf{L}_i^T \begin{bmatrix} ^c\underline{\dot{\mathbf{n}}}_i^1 \\ ^c\underline{\dot{\mathbf{n}}}_i^2 \end{bmatrix} \tag{3}$$

where $\mathbf{N}_i^T$ and $\mathbf{L}_i^T$ are (3×6) matrices [15]. Combining (3) with (1) or (2), we found:

$$\mathbf{H}_i^T \begin{bmatrix} ^c\underline{\dot{\mathbf{n}}}_i^1 \\ ^c\underline{\dot{\mathbf{n}}}_i^2 \end{bmatrix} = \mathbf{M}_i^{T\,c}\boldsymbol{\tau}_c \tag{4}$$

where $\mathbf{H}_i = \mathbf{N}_i$ and $\mathbf{M}_i = \mathbf{M}_{ui}$ in the case of a leg-direction-based controller [1] while $\mathbf{H}_i = [\mathbf{N}_i \ \mathbf{L}_i]$ and $\mathbf{M}_i = \mathbf{M}_{uhi}$ in the case of a line-based controller [15].

Matrices $\mathbf{M}_i^T$ being rank-deficient, in order to obtain the end-effector twist $^c\boldsymbol{\tau}_c$ as a function of the vectors $^c\underline{\dot{\mathbf{n}}}_i^j$, a set of m legs must be observed. By considering the observation of m legs and stacking their equations (4), it comes:

$$\mathbf{H}^{T\,c}\underline{\dot{\mathbf{n}}} = \mathbf{M}^{T\,c}\boldsymbol{\tau}_c \tag{5}$$

where $^c\underline{\dot{\mathbf{n}}} = [^c\underline{\dot{\mathbf{n}}}_1^{1\,T}, {}^c\underline{\dot{\mathbf{n}}}_1^{2\,T}, ..., {}^c\underline{\dot{\mathbf{n}}}_1^{m\,T}, {}^c\underline{\dot{\mathbf{n}}}_1^{m\,T}]^T$, $\mathbf{H}^T$ is a block-diagonal matrix containing the matrices $\mathbf{H}_i^T$ and $\mathbf{M}^T = [\mathbf{M}_1, ..., \mathbf{M}_m]^T$ is of full rank if enough legs are observed (except in the singularities of the hidden robot, as shown in [5]). Then, by using the pseudo-inverse $\mathbf{M}^{T+} = (\mathbf{M}\mathbf{M}^T)^{-1}\mathbf{M}$ of the matrix $\mathbf{M}^T$, we found the relation

$$^c\boldsymbol{\tau}_c = \mathbf{S}^{T\,c}\underline{\dot{\mathbf{n}}}, \text{ with } \mathbf{S}^T = \mathbf{M}^{T+}\mathbf{H}^T = (\mathbf{M}\mathbf{M}^T)^{-1}\mathbf{M}\mathbf{H}^T \tag{6}$$

on which the visual servoing approach is finally based (see [7] for more details).

3 Control-based design of the five-bar mechanism

3.1 Controller-based robot performance

Robots require certain performance to be certified in a given workspace. One of them is the end-effector accuracy.

For a parallel robot controlled with usual encoder-based approaches [12], it is known that the end-effector accuracy is worsen near Type 2 singularities [10], i.e. singularities of the inverse Jacobian matrix $\mathbf{J}_{inv}$. Considering a very simple error model based on the first-order approximation of the geometric model, taking into account only errors $\delta\mathbf{q}$ on the encoder measurements as usual encoder-based controllers did, we have [13]:

$$\delta\mathbf{x} = \mathbf{J}_{inv}^{-1}\delta\mathbf{q} \qquad (7)$$

where $\delta\mathbf{x}$ is the error on the end-effector pose. $\delta\mathbf{x}$ being proportional to $1/\det(\mathbf{J}_{inv})$, for given errors $\delta\mathbf{q}$ the norm of $\delta\mathbf{x}$ considerably grows near Type 2 singularities.

For a parallel robot controlled with leg-based visual servoing approach, the end-effector accuracy is worsen near singularities of the matrix $\mathbf{M}^T$ [4]. Again, considering a very simple error model taking into account only errors $\delta\underline{\mathbf{n}}$ on the observation as leg-based controllers did, we have:

$$\delta\mathbf{x} = \mathbf{S}^T\delta\underline{\mathbf{n}} \qquad (8)$$

$\delta\mathbf{x}$ being proportional to $1/\det(\mathbf{MM}^T)$, for given errors $\delta\underline{\mathbf{n}}$ the norm of $\delta\mathbf{x}$ considerably grows near singularities of the matrix $\mathbf{M}^T$ where $\det(\mathbf{MM}^T)$ is near zero.

Singularities of the matrix $\mathbf{M}^T$ can be found by finding the Type 2 singularities of a virtual robot which is hidden into the controller. As explained in [5], the hidden robot is a proper robot architecture able to perform the same motions as the real robot, but with different set of actuated joints. These virtually actuated joints are linked no more to the real actuator positions $\mathbf{q}$ but to the measurements of the observed link configurations characterized by ${}^c\underline{\mathbf{u}}_i$ or (${}^c\underline{\mathbf{u}}_i$, ${}^c\mathbf{h}_i$). As shown in [15], the hidden robots associated with the visual servoing approaches based on ${}^c\underline{\mathbf{u}}_i$ or (${}^c\underline{\mathbf{u}}_i$, ${}^c\mathbf{h}_i$) applied on a five-bar mechanism (a $\underline{RR}RR\underline{R}$ robot[2], Fig. 2(a)) are the architectures depicted in Figs. 2(b) and 2(c). For direction-based controller, this is a $\Pi\underline{RR}R\Pi$ robot (Fig. 2(b)) while it is a $\underline{RR}PRP\underline{RR}$ robot in the line-based controller (Fig. 2(c)). It should be mentioned that:

- lengths $\ell_{A_iB_i}$ (ℓ_{B_iC}, $\ell_{A_1A_2}$, resp.) are equal for all robots (Fig. 2),
- for the direction-based controller, the only measurements are the leg directions $\underline{\mathbf{u}}_i$: these leg directions can be fixed thanks to the virtual actuators at points B_i mounted on the link B_iD_i in Fig. 2(b), all other joints being passive,
- for the line-based controller, the only measurements are the leg Plücker coordinates (${}^c\underline{\mathbf{u}}_i$, ${}^c\mathbf{h}_i$): these coordinates can be fixed thanks to the virtual actuators at points A_i and B_i in Fig. 2(c), all other joints being passive,
- Type 2 singularities appear when $\underline{\mathbf{u}}_1//\underline{\mathbf{u}}_2$ for the real five-bar mechanism and the $\underline{RR}PRP\underline{RR}$ robot while singularities of the $\Pi\underline{RR}R\Pi$ robot are when $\underline{\mathbf{v}}_1//\underline{\mathbf{v}}_2$.

For reason of brevity, the reader is referred to [5] in order to get more information about the hidden robot models and the ways to find them.

Based on these considerations, it should be understood that, in order to have good accuracy performance when leg-based visual controllers are used, (**1**) singularities of the hidden robot models must be avoided in the robot operational workspace, as well as the singularities of the real robots and (**2**) positioning errors come not from the encoder errors $\delta\mathbf{q}$ but from the observation errors $\delta\underline{\mathbf{n}}$. When designing a robot that will be controlled through leg-based visual servoing approaches, these two items must be taken into consideration in order to have the best robot performance.

---

[2] In what follows, R stands for revolute joint while P is for prismatic joint. Moreover, Π is for a parallelogram joint [6]. If the letter is underlined, the joint is actuated. It is passive if not.

(a) The five-bar mechanism

(b) The hidden robot model associated with the direction $^c\underline{\mathbf{u}}_i$-based controller

(c) The hidden robot model associated with the line ($^c\underline{\mathbf{u}}_i$, $^c\mathbf{h}_i$)-based controller
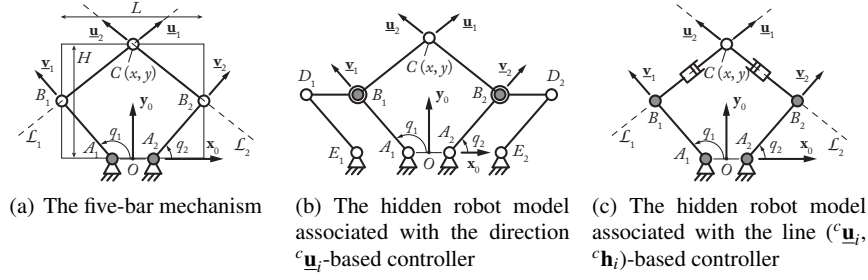
Fig. 2 The five-bar mechanism and its associated hidden robot models (actuators are in gray).

3.2 Optimal design process

In order to see the effect on the robot accuracy when it is controlled using leg-based visual servoing approaches but that the hidden robot models are not taking into account, we propose to optimize the design of a five-bar mechanism for the following objective and constraints[3] which are similar to those proposed in [9]:

- **Objective:** the robot footprint should be minimal. This footprint is characterized by the rectangular area $A = LH$ in which the robot is included when the links A_iB_i and B_iC are perpendicular (Fig. 2(a)),
- **Constraints:** the robot must have a dexterous regular workspace [13] of rectangular shape with dimensions along $\mathbf{x}_0$ of $\ell_{W_{x0}} = 800$ mm and along $\mathbf{y}_0$ of $\ell_{W_{y0}} = 100$ mm in which the following properties are certified for all robots:

  - no Type 2 singularities of the real robot,
  - knowing the maximum actuated joint velocity taken at $V_{max} = 600$ rpm, the robot end-effector should be able to reach a velocity of 6 m/s in any direction, wherever in the regular dexterous workspace,
  - the static forces exerted into the passive joints are proportional to $1/\sin\xi$, ξ being the angle between the distal links [3]. Consequently, it is decided that $\sin\xi$ should be higher than 0.1 to avoid excessive efforts in the joints.

  In addition, the following constraints depend on the controller type:

- **for encoder-based control:** knowing the resolution of the motor encoders (taken as $\delta q = 28000$ pt/rev), the resolution on the platform position $\delta\mathbf{x}$ computed with (7) should be lower than 0.5 mm
- **for leg-based visual control:** here, a camera with 2336×1728 pixels is taken as a sensor. The following constraints must be verified:

  - no Type 2 singularities of the considered hidden robot model,
  - the end-effector is within the image frame and thus the legs can be observed,

---

[3] In what follows, values for the motor and encoders specifications are those of the IRSBot-2 prototype [8]. Values for the camera are those of a 4CXP MC408X Mikroton camera of IRCCyN.

Table 1 Optimal design parameters and value of the objective function

Encoder-based controller		Direction-based controller ($^c\underline{\mathbf{u}}_i$)		Line-based controller ($^c\underline{\mathbf{u}}_i$, $^c\mathbf{h}_i$)	
ℓ_0 [m]	0.1071	ℓ_0 [m]	0.1092	ℓ_0 [m]	0.1074
ℓ_1 [m]	0.2219	ℓ_1 [m]	0.2291	ℓ_1 [m]	0.2443
ℓ_2 [m]	0.3863	ℓ_2 [m]	0.3750	ℓ_2 [m]	0.3568
y_c [m]	N/A	y_c [m]	0.4340	y_c [m]	0.3274
z_c [m]	N/A	z_c [m]	0.5908	z_c [m]	0.6596
A [m^2]	0.1144	A [m^2]	0.1156	A [m^2]	0.1124

- knowing the resolution of the camera (taken as 1 pixel), the resolution on the platform position $\delta\mathbf{x}$ computed with (8) should be lower than 0.5 mm (relation between the camera frame, in which the vectors $\delta\underline{\mathbf{n}}$ are expressed in (8), and the pixel frame are given in [1]).

The general procedure to solve an optimal design problem for a robot was described in [9], in which the way to compute the size of the dexterous workspace is given. We use the same procedure which is based on the following formulation of the design optimization problem:

$$\begin{aligned} \text{minimize} \quad & A = LH \\ \text{over} \quad & \mathbf{x} \\ \text{subject to} \quad & \ell_{W_x} > \ell_{W_{x0}} \text{ and } \ell_{W_y} > \ell_{W_{y0}} \end{aligned} \qquad (9)$$

where ℓ_{W_x} and ℓ_{W_y} are the dimensions along $\mathbf{x}_0$ and $\mathbf{y}_0$ of the rectangular dexterous workspace in which all constraints are satisfied, and

- $\mathbf{x} = [\ell_0 \ \ell_1 \ \ell_2]$ in encoder-based design procedure, with $\ell_0 = \ell_{A_1A_2}$, $\ell_1 = \ell_{A_1B_1} = \ell_{A_2B_2}$ and $\ell_2 = \ell_{B_1C} = \ell_{B_2C}$,
- $\mathbf{x} = [\ell_0 \ \ell_1 \ \ell_2 \ y_c \ z_c]$ in control-based design procedures, where y_c and z_c are the coordinate of the camera center along $\mathbf{y}_0$ and $\mathbf{z}_0$, respectively.

It should be mentioned that, in order to reduce the number of decision variables in the optimization problem, we decided to fix the orientation of the camera plane so that it was parallel to the plane $(\mathbf{x}_0 O \mathbf{y}_0)$. Moreover, due to the symmetry in the robot design, the coordinate x_c of the camera center along $\mathbf{x}_0$ was fixed at $x_c = 0$ m. Finally, we fixed the radius of the observed cylinders at 4 cm.

3.3 Results of the optimization process

The previous optimization algorithm was applied for the design of the mentioned five-bar mechanism and the optimal design parameters, as well as the value of the objective function, are given in Tab. 1 as a function of the used control approach.

All results are very close, but the difference is not negligible. For instance, let us consider that a leg-direction-based controller is used in order to control the robot designed with the encoder-based optimal design procedure. Figure 3 shows the robot to scale, with the singularity loci of the hidden robot associated with the used
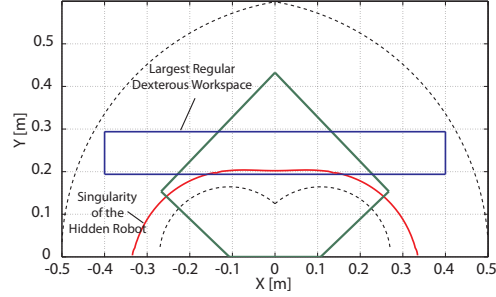
Fig. 3 Largest regular dexterous workspace and hidden robot singularities for the encoder-optimised architecture

controller. We can see that the singularity loci are included in the robot dexterous workspace.

In order to see the effect of the presence of singularities, simulations were performed in a connected ADAMS-Simulink environment similar as the one developed in [15]. We simulated a measurement noise of one pixel for the observation, and we asked the robot to go to the position $\{x = 0.15 \text{ m}, y = 0.2 \text{ m}\}$ which is, for this robot, near a singularity of the hidden robot model but in the dexterous workspace of the real robot. Resulting position accuracy for the end-effector is about 1.2 mm, which is more than twice higher than the desired accuracy. We did the same experiment, but with the robot optimized for the used controller. Accuracy was lower than the desired 0.5 mm.

All these results showed the importance of taking into account the controller at the earliest design stage so that it is possible to get the best performance for the controlled robot.

4 Conclusion

In the present paper, we introduced a design methodology which took into account the specificities of the controller used to servo the robot motions. We showed that, in order to get the best accuracy performance of a robot, it is necessary to extract control-based performance indices from the control scheme.

We optimized the design of five-bar mechanism using a classical design methodology. The robot was then compared with other designs which are the result of the new methodology, taking into account the nature of the desired control scheme through the incorporation of control-based performance indices into the optimization process. Simulation results showed that, even though the latter designs might have a bigger footprint, they exhibited better accuracy performance when controlled using exteroceptive sensors.

References

1. Andreff, N., Dallej, T., Martinet, P.: Image-based visual servoing of Gough-Stewart parallel manipulators using legs observation. International Journal of Robotics Research **26**(7), 677–687 (2007)
2. Andreff, N., Martinet, P.: Vision-based kinematic modelling of some parallel manipulators for control purposes. In: Proceedings of EuCoMeS, the First European Conference on Mechanism Science. Obergurgl, Austria (2006)
3. Briot, S., Glazunov, V., Arakelian, V.: Investigation on the effort transmission in planar parallel manipulators. ASME Journal of Mechanisms and Robotics **5**(1) (2013)
4. Briot, S., Martinet, P.: Minimal representation for the control of Gough-Stewart platforms via leg observation considering a hidden robot model. In: Proceedings of the 2013 IEEE International Conference on Robotics and Automation (ICRA 2013), pp. 4653–4658. Karlsruhe, Germany (2013)
5. Briot, S., Martinet, P., Rosenzveig, V.: The hidden robot: an efficient concept contributing to the analysis of the controllability of parallel robots in advanced visual servoing techniques. IEEE Transactions on Robotics **31**(6), 1337–1352 (2015)
6. Caro, S., Khan, W., Pasini, D., Angeles, J.: The rule-based conceptual design of the architecture of serial Schoenflies-motion generators. Mechanism and Machine Theory **45**(2), 251–260 (2010)
7. Chaumette, F., Huchinson, S.: Handbook of robotics, chap. 24: Visual Servoing and Visual Tracking, pp. 563–583. Springer (2008)
8. Germain, C., Briot, S., Caro, S., Izard, J., Baradat, C.: Task-oriented design of a high-speed parallel robot for pick-and-place operations. In: Proceedings of the Task-based Optimal Design of Robots (ICRA 2014 WS), 2014 IEEE International Conference on Robotics and Automation (ICRA 2014). Hong Kong, China (2014)
9. Germain, C., Caro, S., Briot, S., Wenger, P.: Optimal Design of the IRSBot-2 Based on an Optimized Test Trajectory. In: Proceedings of the ASME 2011 International Design Engineering Technical Conferences and Computers and Information in Engineering Conference (IDETC/CIE 2013). Portland, OR, USA (2013)
10. Gosselin, C., Angeles, J.: Singularity analysis of closed-loop kinematic chains. IEEE Transactions on Robotics and Automation **6**(3), 281–290 (1990)
11. Hollerbach, J., Khalil, W., Gautier, M.: Handbook of Robotics, chap. 14: Model Identification, pp. 321–344. Springer (2008)
12. Khalil, W., Dombre, E.: Modeling, Identification and Control of Robots. Hermès Penton London (2002)
13. Merlet, J.: Parallel Robots, 2nd edn. Springer (2006)
14. Traslosheros, A., Sebastian, J., Angel, L., Roberti, F., Carelliz, R.: Visual servoing of a parallel robot system. In: IEEE International Symposium on Intelligent Signal Processing, pp. 1–6 (2007)
15. Vignolo, A., Briot, S., Martinet, P., Chen, C.: Comparative analysis of two types of leg-observation-based visual servoing approaches for the control of the five-bar mechanism. In: Proceedings of the 2014 Australasian Conference on Robotics and Automation (ACRA 2014). University of Melbourne, Australia (2014)